Enhanced ethanol production inside carbon-nanotube reactors containing catalytic particles

XIULIAN PAN, ZHONGLI FAN, WEI CHEN, YUNJIE DING, HONGYUAN LUO AND XINHE BAO*

State Key Laboratory of Catalysis, Dalian Institute of Chemical Physics, The Chinese Academy of Sciences, Dalian 116023, PR China
*e-mail: xhbao@dicp.ac.cn

Published online: 21 May 2007; doi:10.1038/nmat1916

Carbon nanotubes (CNTs) have well-defined hollow interiors and exhibit unusual mechanical and thermal stability as well as electron conductivity[1]. This opens intriguing possibilities to introduce other matter into the cavities[2–5], which may lead to nanocomposite materials with interesting properties or behaviour different from the bulk[6–8]. Here, we report a striking enhancement of the catalytic activity of Rh particles confined inside nanotubes for the conversion of CO and H_2 to ethanol. The overall formation rate of ethanol (30.0 mol mol^{-1}Rh h^{-1}) inside the nanotubes exceeds that on the outside of the nanotubes by more than an order of magnitude, although the latter is much more accessible. Such an effect with synergetic confinement has not been observed before in catalysis involving CNTs. We believe that our discovery may be of a quite general nature and could apply to many other processes. It is anticipated that this will motivate theoretical and experimental studies to further the fundamental understanding of the host–guest interaction within carbon and other nanotube systems.

With soaring oil prices and dwindling resources, ethanol and other alternative energy sources have moved into the spotlight in recent years as clean, sustainable and transportable fuel alternatives[9]. This has sparked rapid global growth of industries producing ethanol on large scales by fermentation of agricultural carbohydrates such as cane sugar and cornstarch. However, it seems that nature cannot provide both food and fuel for a still growing and increasingly energy-hungry world population in the near future[9,10]. Syngas (a mixture of CO and H_2) conversion over Rh-based catalysts to ethanol[11] offers a good alternative because other C2 oxygenate by-products (for example, acetaldehyde and acetic acid) can be readily hydrogenated to ethanol, and syngas can be conveniently manufactured from natural gas and coal at present and from biomass in the future. On the other hand, carbon nanotubes (CNTs) have been widely studied as supports for nanoscopic metal catalysts[12–14], although those were generally deposited on the outer CNT surface. The few experimental examples of catalytic reactions inside CNTs were liquid-phase hydrogenations, which showed moderate improvement of selectivity or activity with respect to conventional catalysts[15,16]. Recently, it has been shown that the autoreduction of iron oxide nanoparticles within CNT channels in an inert gas atmosphere is significantly facilitated and sensitive to the CNT inner diameter, whereas the oxidation of metal particles is retarded compared with that of particles located on the outer CNT surface[17–19]. We believe that the C2 oxygenate formation from syngas inside Rh-loaded CNTs reported here is the first example

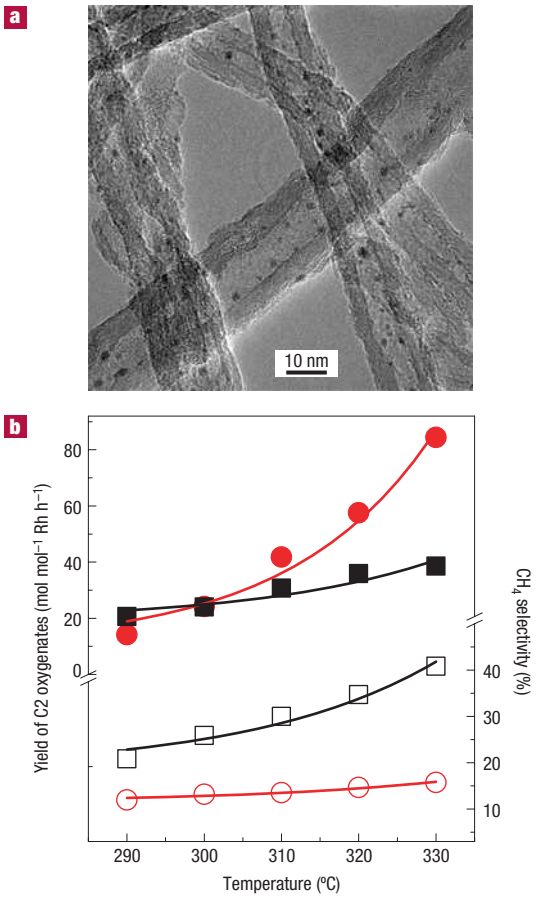

Figure 1 TEM image and catalytic performance of RMLF-in-CNTs in C2 oxygenate formation. a, TEM image of the RMLF-in-CNTs catalyst. **b**, Yield of C2 oxygenate and selectivity to CH_4, in comparison with the RMLF-on-SiO_2 catalyst. Circles: RMLF-in-CNTs; squares: RMLF-on-SiO_2. The filled symbols denote the C2 oxygenate yield and the open symbols denote the selectivity of CH_4.

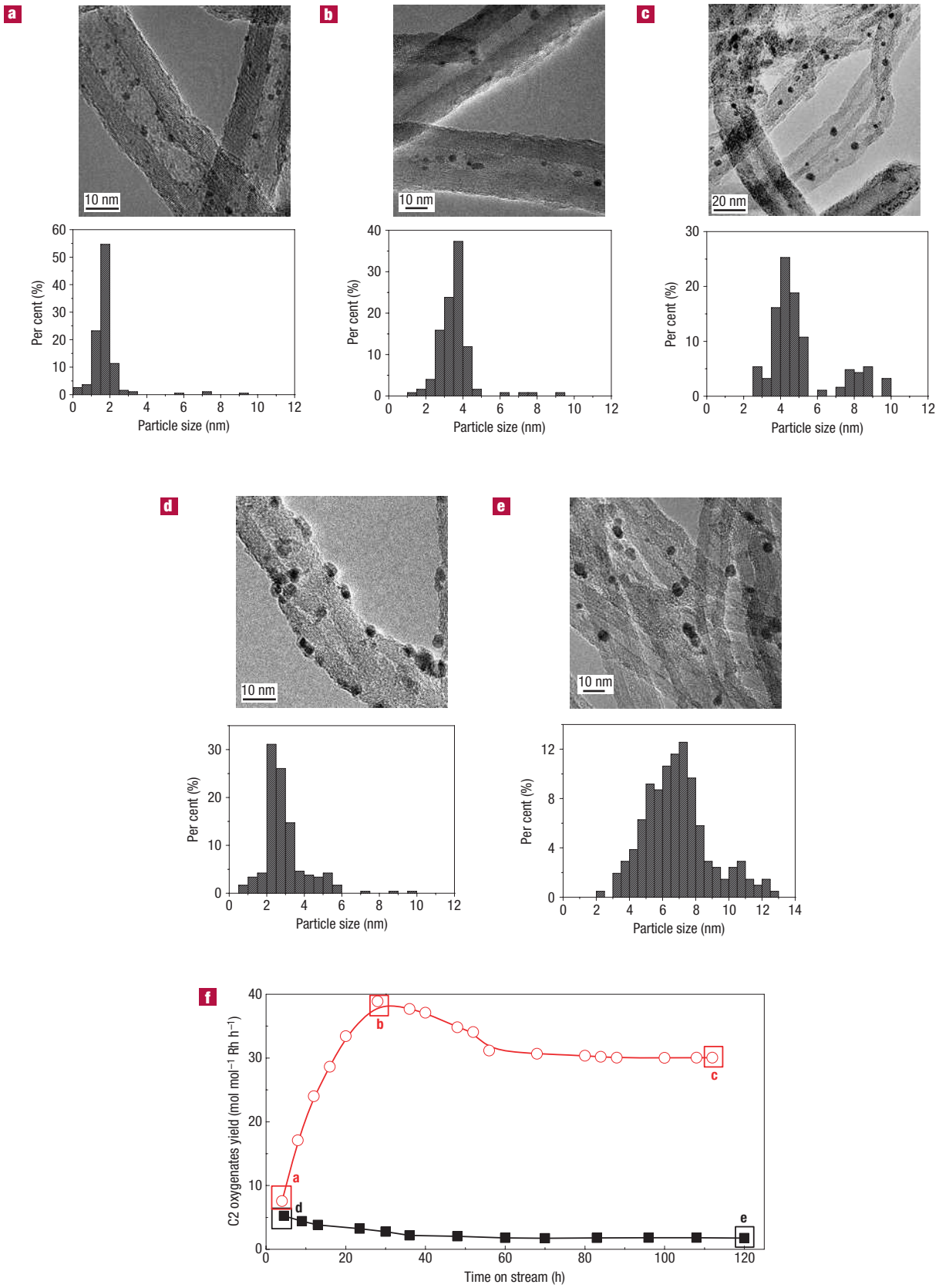

Figure 2 TEM images and particle size distribution of catalysts and their C2 oxygenate formation activities. a–c, Fresh RM-in-CNTs catalyst (**a**), that after 28 h (**b**) and after 112 h (**c**) of reaction. **d**,**e**, Fresh RM-out-CNTs catalyst (**d**) and that after 120 h of reaction (**e**). **f**, C2 oxygenate formation activities as a function of time on stream. Reaction temperature: 320 °C.

where the activity and selectivity of a metal-catalysed gas-phase reaction benefits significantly from proceeding inside a nanosized CNT reaction vessel.

Active components of Rh and Mn with Li and Fe as the additives in a weight ratio of 1:1:0.075:0.05 were introduced into the CNT lumen (4–8 nm inner diameter and 250–500 nm length) by a wet-chemistry method using the capillary forces of the tubes[4,20] aided by ultrasonic treatment and stirring. Thus, a catalyst labelled as RMLF-in-CNTs with a nominal 1.2 wt% Rh loading was obtained. Over 80% of the particles were homogeneously distributed inside the channels with the rest on the outer surface, as indicated by transmission electron microscopy (TEM) (Fig. 1a). For comparison, the same composition of metals was dispersed on a conventional silica support to obtain an RMLF-on-SiO_2 catalyst. Figure 1b shows that the activity of RMLF-in-CNTs is significantly improved, particularly at higher temperatures. The C2 oxygenates yield (containing up to 76% ethanol, see Supplementary Information, Table S1 and Fig. S2 for detailed selectivities) at 330 °C is 84.4 mol $mol^{-1}Rh\,h^{-1}$, more than twice that on RMLF-on-SiO_2. More remarkably, the selectivity to the undesired by-product CH_4 is reduced to about 15% from 41% over RMLF-on-SiO_2 (ref. 21). Furthermore, no obvious deactivation of RMLF-in-CNTs is observed over a period of 180 h.

To ascertain the effect of the CNT channels, we deposited a simplified metal mixture of 5% Rh and 5% Mn both inside and outside the CNTs, denoted as RM-in-CNTs and RM-out-CNTs, respectively. Supplementary Information, Fig. S1a–g shows that the RhMn particles are uniformly distributed inside the tubes in the fresh RM-in-CNTs. Figure 2a shows that over 75% of the particles are in the size range of 1–2 nm. This catalyst yields 7.5 mol C2 oxygenates $mol^{-1}Rh\,h^{-1}$ (open circles in Fig. 2f). The activity increases steeply and reaches a maximum value of 38.9 mol $mol^{-1}Rh\,h^{-1}$ after about 28 h. TEM shows a slight aggregation of the particles, but they are still fairly uniform and the most abundant ones are 3–4 nm in size (Fig. 2b). Then the activity gradually levels off after 60 h at a steady production rate of 30.0 mol $mol^{-1}Rh\,h^{-1}$ (Fig. 2f). After 112 h of reaction, the particle size within the channels is found to be about 4–5 nm, in accordance with the average inner diameter of the CNTs, whereas those on the outer surface have grown to about 8 nm (Fig. 2c). Obviously, the CNT channels have restricted the growth of the particles inside, and the 3–4 nm size corresponds to the maximum activity, in agreement with earlier studies on SiO_2-supported Rh catalysts[22].

However, the RM-out-CNTs catalyst (Fig. 2d) gives only an initial C2 oxygenate yield of 5.3 mol $mol^{-1}Rh\,h^{-1}$ (filled squares in Fig. 2f), although the particle size of RM-out-CNTs (2–4 nm) is also in the optimal range. The activity of RM-out-CNTs decreases continuously from the initial value with time on stream. The C2 oxygenate yield is 16 times lower than that on RM-in-CNTs after 120 h of reaction. The contribution of the outer particles (20%) of RM-in-CNTs can be estimated to be only ~1% of the total yield of C2 oxygenates using the yield of RM-out-CNTs. This demonstrates a remarkable enhancement of the activity for the particles inside compared with those outside the CNTs. This behaviour is even more surprising considering that diffusion of reactants and products in and out of the nanotubes should hinder the reaction to some extent with respect to that on the freely accessible outer CNT surface. Obviously the significantly different catalytic activities of RM-in-CNTs and RM-out-CNTs cannot be related to the number of particles because the loadings of active components and the size of the catalytic particles in both samples are similar. Furthermore, the exclusive contribution of the geometrical effect of the channel structure on the unique catalytic property inside the CNTs is ruled out by a comparison experiment with mesoporous silica SBA-15 as a support, which yields a much poorer catalytic performance than RMLF-in-CNTs (see Supplementary Information, Fig. S3), although SBA-15 possesses a similar morphology to CNTs with respect to the channel diameter (6–7 nm) and length (300–600 nm), and thus can provide a similar dimensional confinement for the metal particles.

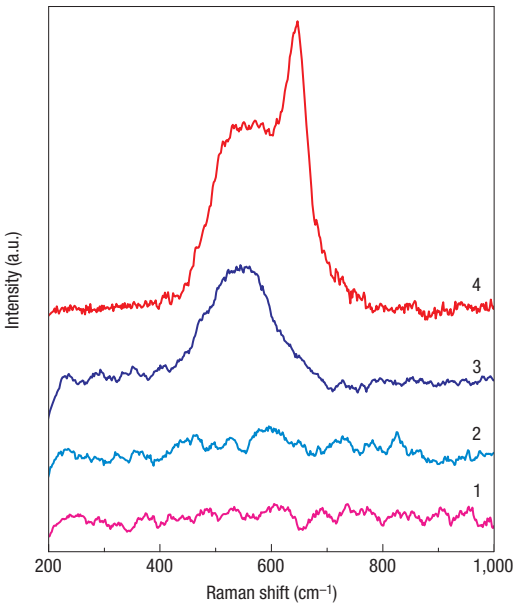

Figure 3 Raman spectra. 1: Reduced RM-in-CNTs; 2: reduced RM-out-CNTs; 3: CO-adsorbed RM-out-CNTs; 4: CO-adsorbed RM-in-CNTs.

Our preliminary Raman spectroscopy data indicate that an interaction between the CNT surface and metal particles could play a crucial role in the improvement of catalytic activity inside CNTs. Figure 3 shows that no obvious Raman bands are observed for both RM-in-CNTs and RM-out-CNTs after *in situ* reduction in hydrogen, although it is widely accepted that the MnO is unlikely to be fully reduced to metallic Mn in RhMn catalysts[22–25]. On subsequent exposure to CO at room temperature, the Raman spectrum of RM-in-CNTs shows two new bands at 550 and 640 cm^{-1}, whereas that of RM-out-CNTs shows only one band at 540 cm^{-1}. The 540−550 cm^{-1} features can be assigned to ν_{Rh-CO} because Rh–CO modes have been reported in the range of 540−600 cm^{-1} for Rh carbonyl complexes[26,27].

The 640 cm^{-1} band on the CO-treated RM-in-CNTs indicates the presence of ν_{Mn-O} modes inside the CNTs, as demonstrated by a similar feature observed in bulk MnO[28] and M-in-CNTs (see Supplementary Information, Fig. S4). It is known that the exterior surfaces of CNTs are electron-rich, whereas the interior ones are electron-deficient[17,29,30], which could influence metal and metal oxide particles in contact with either surface. Thus, the oxophilic Mn inside CNTs could attract the O of CO adsorbed on adjacent Rh sites leading to tilted adsorption of CO with the C atom bonding to a Rh atom and the O bonding to a Mn atom. The 640 cm^{-1} band observed here probably indicates an almost completed dissociation. Such a tilted adsorption of CO on RhMn catalysts bridging Rh and Mn sites facilitates the dissociation of CO and hence increases the C2 oxygenate formation activity, as suggested previously[24,25]. In contrast, the electron-rich exterior surface reduces the tendency of Mn to accept oxidic CO donor electrons. Consequently, the dissociation of CO is retarded on the CNT outer surface, leading to a lower formation rate of C2 oxygenates. In addition, the higher ν_{Rh-CO} frequency (550 cm^{-1}) inside the CNTs suggests a

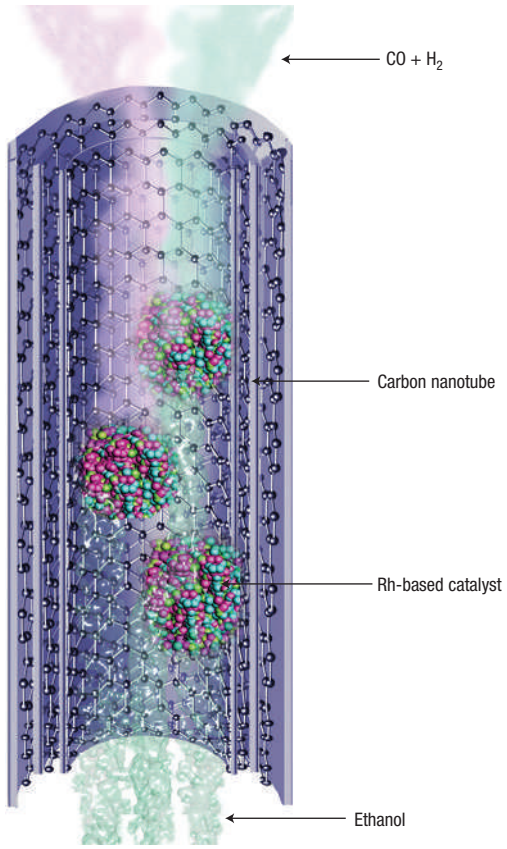

Figure 4 Schematic diagram showing ethanol production from syngas inside Rh-loaded carbon nanotubes. The black spheres denote carbon atoms, which form the graphene layers of the carbon nanotubes. The streams in light orange and green entering the nanotubes indicate the gas mixture of CO and H_2, respectively. The three stacks of small spheres in rose, blue, green and red inside the tubes represent catalyst particles that may comprise more than one component. The streams in light cyan tailing behind the catalyst particles along the axis of the nanotubes represent ethanol.

stronger Rh–CO bonding strength, which is another sign of easier dissociation of the C–O bond compared with RM-out-CNTs.

Figure 4 schematically summarizes the ethanol production inside a carbon-nanotube reactor containing catalytic particles. The enhancement of the activity by more than an order of magnitude inside the CNTs compared with the conversion on the more accessible outer surface can be attributed to the confinement of the nanoparticles within the CNTs, leading to the peculiar interaction of the interior nanotube surface with the metal particles, which benefits the dissociation of CO. Theoretical studies on non-catalytic gas-phase reactions have prefigured that confinement within small channels could increase the density of reactants[31], and hence create a locally higher pressure, which will favour syngas conversion to C2 oxygenates in the present case. In fact, a much higher intensity of the H_2 desorption peak is observed on RM-in-CNTs than that on RM-out-CNTs during temperature-programmed desorption experiments (see Supplementary Information, Fig. S5), indicating a higher concentration of active hydrogen species inside the CNTs, which will further supplement the hydrogenation rate[32]. It is generally agreed that the formation of C2 oxygenates involves the dissociative adsorption of CO, hydrogenation of carbon species and insertion of the molecular CO adsorbed on the catalyst surface into CH_x species, followed by hydrogenation. Thus, both the facilitated dissociation/activation of CO and increased hydrogenation rate lead to a significant increase in the overall yield of C2 oxygenates. This synergetic confinement effect of metal nanoparticles inside CNTs could lead to new advances and applications pertaining to functional materials in electronic, magnetic and catalytic fields, and related processes.

METHODS

CATALYST PREPARATION

CNTs (inner diameter 4–8 nm and outer diameter 10–20 nm) were purchased from Chengdu Organic Chemicals. Raw CNTs were refluxed in HNO_3 (68 wt%) for 14 h at 140 °C in an oil bath. Then the mixture was filtered and washed with deionized water, followed by drying at 60 °C for 12 h. The purity of the CNTs obtained was 99.9%, containing about 10 p.p.m. iron detected by X-ray fluorescence. TEM indicated that all of the CNTs had open ends with a length of 250–500 nm. The CNTs were then immersed into an aqueous solution of precursor salts of Rh, Mn, Li and Fe under stirring to prepare RMLF-in-CNTs. The aqueous solution was drawn into the CNT channels by capillary forces aided by ultrasonic treatment and stirring. The ultrasonic treatment facilitated the filling of the CNT channels with precursor solution during the impregnation. A carefully controlled slow drying process was carried out. First, the mixture was stirred at room temperature overnight, followed by heating in air to 120 °C at 1 °C min^{-1} and held for 10 h. In this way, the catalyst components were homogeneously distributed inside the CNT lumen along the tube axis.

For the preparation of RM-out-CNTs, nanotubes with closed ends were used, which were obtained by refluxing raw CNTs in 6 M nitric acid (37 wt%) at 110 °C for 5 h. This milder treatment removed amorphous carbon while keeping the caps intact. Scanning across several specimens by transmission electron microscopy (TEM), we did not observe nanotubes with open ends. Then an impregnation procedure was carried out to disperse the active components on the outer surface of these nanotubes.

SBA-15 was purchased from Jilin University HighTech. RMLF-in-SBA was prepared in the same manner as RMLF-in-CNTs. These two catalysts as well as RMLF-on-SiO_2 had the same metal composition. The latter catalyst was prepared by impregnation of SiO_2, which was obtained from Qingdao Haiyang Chemical Group, with an average pore size of 20 nm.

REACTION AND ANALYSIS OF REACTION PRODUCTS

Reactions were carried out in a flow-type fixed-bed reactor. A diagram of the reaction rig is shown in Supplementary Information, Fig. S6. The standard conditions were 3 MPa, $H_2/CO = 2$ (molar ratio), gas hourly space velocity = 12,000 h^{-1}, catalyst charge = 0.3 g. Before the reaction, the catalyst was reduced *in situ* at 350 °C in a H_2 stream (50 ml min^{-1}) for 2 h. The effluent passed through a condenser filled with deionized water. The oxygenates collected in the condenser were analysed offline by Varian CP-3800 gas chromatography using a flame ionization detector and the tail gas was analysed online using a thermal conductivity detector.

TEM CHARACTERIZATION

Measurements were carried out on an FEI Tecnai F30 microscope operated at an accelerating voltage of 300 kV.

RAMAN SPECTROSCOPY

Spectra were obtained with a LabRam I confocal microprobe Raman instrument (Dilor). The excitation wavelength was 632.8 nm. Before CO adsorption, the sample was reduced *in situ* in a flowing H_2 stream at 350 °C for 2 h, followed by purging in Ar for 30 min at this temperature, and then cooled to room temperature in Ar. The adsorption of CO was allowed for 30 min at room temperature. Then the spectrum was recorded in Ar.

Received 30 January 2007; accepted 13 April 2007; published 21 May 2007.

References

1. Dai, H. Carbon nanotubes: Synthesis, integration, and properties. *Acc. Chem. Res.* **35**, 1035–1044 (2002).
2. Ajayan, P. M. *et al.* Opening carbon nanotubes with oxygen and implications for filling. *Nature* **362**, 522–525 (1993).
3. Seraphin, S., Zhou, D., Jiao, J., Withers, J. C. & Loutfy, R. Yttrium carbide in nanotubes. *Nature* **362**, 503 (1993).
4. Tsang, S. C., Chen, Y. K., Harris, P. J. F. & Green, M. L. H. A simple chemical method of opening and filling carbon nanotubes. *Nature* **372**, 159–162 (1994).

5. Guerret-Plécourt, C., Bouar, Y. L., Loiseau, A. & Pascard, H. Relation between metal electronic structure and morphology of metal compounds inside carbon nanotubes. *Nature* **372**, 761–765 (1994).
6. Koga, K., Gao, G. T., Tanaka, H. & Zeng, X. C. Formation of ordered ice nanotubes inside carbon nanotubes. *Nature* **412**, 802–805 (2001).
7. Sloan, J. *et al.* Metastable one-dimensional $AgCl_{1-x}I_x$ solid-solution wurzite tunnel crystals formed within single-walled carbon nanotubes. *J. Am. Chem. Soc.* **124**, 2116–2117 (2002).
8. Mühl, T. *et al.* Magnetic properties of aligned Fe-filled carbon nanotubes. *J. Appl. Phys.* **93**, 7894–7896 (2003).
9. Farrell, A. E. *et al.* Ethanol can contribute to energy and environmental goals. *Science* **311**, 506–508 (2006).
10. Deluca, T. H. Looking at biofuels and bioenergy. *Science* **312**, 1743–1744 (2006).
11. Bhasin, M. M. & O'Connor, G. L. Procede de preparation selective de derives hydrocarbones oxygenes a deux atomes de carbone. Belgian Patent 824822 (1975).
12. Planeix, J. M. *et al.* Application of carbon nanotubes as supports in heterogeneous catalysis. *J. Am. Chem. Soc.* **116**, 7935–7936 (1994).
13. Yoon, B. & Wai, C. M. Microemulsion-templated synthesis of carbon nanotube-supported Pd and Rh nanoparticles for catalytic applications. *J. Am. Chem. Soc.* **127**, 17174–17175 (2005).
14. Girishkumar, G., Hall, T. D., Vinodgopal, K. & Kamat, P. V. Single wall carbon nanotube supports for portable direct methanol fuel cells. *J. Phys. Chem. B* **110**, 107–114 (2006).
15. Zhang, A. M., Dong, J. L., Xu, Q. H., Rhee, H. K. & Li, X. L. Palladium cluster filled in inner of carbon nanotubes and their catalytic properties in liquid phase benzene hydrogenation. *Catal. Today* **93–95**, 347–352 (2004).
16. Tessonnier, J., Pesant, L., Ehret, G., Ledoux, M. J. & Pham-Huu, C. Pd nanoparticles introduced inside multi-walled carbon nanotubes for selective hydrogenation of cinnamaldehyde into hydrocinnamaldehyde. *Appl. Catal. A* **288**, 203–210 (2005).
17. Chen, W., Pan, X., Willinger, M., Su, D. & Bao, X. Facile autoreduction of iron oxide/carbon nanotube encapsulates. *J. Am. Chem. Soc.* **128**, 3136–3137 (2006).
18. Chen, W., Pan, X. & Bao, X. Tuning of redox properties of iron and iron oxides via encapsulation within carbon nanotubes. *J. Am. Chem. Soc.* (2007, in the press, doi:10.1021/ja0713072).
19. Cao, F. *et al.* Reducing reaction of Fe_3O_4 in nanoscopic reactors of a-CNTs. *J. Phys. Chem. B* **111**, 1724–1728 (2007).
20. Dujardin, E., Ebbesen, T. W., Hiura, H. & Tanigaki, K. Capillarity and wetting of carbon nanotubes. *Science* **265**, 1850–1852 (1994).
21. Yin, H. *et al.* Influence of iron promoter on catalytic properties of Rh−Mn−Li/SiO_2 for CO hydrogenation. *Appl. Catal. A* **243**, 155 (2003).
22. Hanaoka, T. *et al.* Ethylene hydroformylation and carbon monoxide hydrogenation over modified and unmodified silica supported rhodium catalysts. *Catal. Today* **58**, 271–280 (2000).
23. de Jong, K. P., Glezer, J. H. E., Kuipers, H. P. C. E., Knoester, A. & Emeis, C. A. Highly dispersed Rh/SiO_2 and Rh/MnO/SiO_2 catalysts: 1. Synthesis, characterization, and CO hydrogenation activity. *J. Catal.* **124**, 520–529 (1990).
24. Trevino, H., Lei, G. & Sachtler, W. M. H. CO hydrogenation to higher oxygenates over promoted rhodium: Nature of the metal-promoter interaction in RhMn/NaY. *J. Catal.* **154**, 245–252 (1995).
25. Ichikawa, M. & Fukushima, T. Infrared studies of metal additive effects on CO chemisorption modes on SiO_2-supported Rh-Mn, -Ti, and –Fe catalysts. *J. Phys. Chem.* **89**, 1564–1567 (1985).
26. Moigno, D., Callejas-Gaspar, B., Gil-Rubio, J., Werner, H. & Kiefer, W. The metal-carbon bond in vinylidene, carbonyl, isocyanide and ethylene complexes. *J. Organometal. Chem.* **661**, 181–190 (2002).
27. von Ahsen, B. *et al.* Cationic carbonyl complexes of rhodium (I) and rhodium (III): Synthesis, vibrational spectra, NMR studies, and molecular structures of tetrakis(carbonyl) rhodium(I) heptachlorodialuminate and –gallate, $[Rh(CO)_4][Al_2Cl_7]$ and $[Rh(CO)_4][Ga_2Cl_7]$. *Inorg. Chem.* **42**, 3801–3814 (2003).
28. Kapteijn, F. *et al.* Alumina-supported manganese oxide catalysts: I. characterization: effect of precursor and loading. *J. Catal.* **150**, 94 (1994).
29. Haddon, R. C. Chemistry of the fullerenes: The manifestation of strain in a class of continuous aromatic molecules. *Science* **261**, 1545–1550 (1993).
30. Ugarte, D., Chatelain, A. & de Heer, W. A. Nanocapillarity and chemistry in carbon nanotubes. *Science* **274**, 1897–1899 (1996).
31. Santiso, E. E. *et al.* Adsorption and catalysis: The effect of confinement on chemical reactions. *Appl. Surf. Sci.* **252**, 766–777 (2005).
32. Dong, X., Zhang, H., Lin, G., Yuan, Y. & Tsai, K. R. Highly active CNT-promoted Cu−ZnO−Al_2O_3 catalyst for methanol synthesis from $H_2/CO/CO_2$. *Catal. Lett.* **85**, 237–246 (2003).

Acknowledgements

We thank Z. Tian and W. Weng from Xiamen University China for their help with Raman spectroscopy characterization and A. Goldbach for the discussion. We also acknowledge the financial support of the Natural Science Foundation of China and the Ministry of Science and Technology of China.
Correspondence and requests for materials should be addressed to X.B.
Supplementary Information accompanies this paper on www.nature.com/naturematerials.

Competing financial interests

The authors declare no competing financial interests.